Nig. J. Pure and Appl. Sci. Vol. 39 (Issue 1, 2026)
e-ISSN 2756-4045
(C) 2026 Faculty of Physical Sciences and Faculty of Life Sciences, Univ. of Ilorin, Nigeria
www.njpas.com.ng

Synthesis, Spectroscopic Characterization and DFT Analysis of a Pd(II) Complex Derived from a Trifluoromethyl-Substituted Schiff Base Ligand

[1*]Waziri, I., [2*]Wahab, O.O., [3]Isa, B., [4]Liman, I.A., [5]Yurari, M.A. and [1]Bute, M.S.

[1]Department of Pure and Applied Chemistry, University of Maiduguri, P.M.B. 1069, Maiduguri, Borno State Nigeria

[2]Department of Chemistry, Nigerian Defence Academy, P.M.B. 2109, Afaka, Kaduna, Nigeria

[3]Department of Chemistry, Kashim Ibrahim University, Maiduguri, Borno State, Nigeria

[4]Nigerian Army Institute of Science Education and Technology Ilorin, P.M.B. 1410, Ilorin, Kwara State, Nigeria

[5]Department of Chemistry, Yobe State University, Damaturu, Yobe state, Nigeria

Date Received: 01-12-2025
Date Accepted: 01-02-2026
DOI: https://doi.org/10.48198/NJPAS/25.B46

ABSTRACT

Herein, a new Schiff base ligand, *(E)-2-[(4-trifluoromethylbenzylidene)amino]phenol (*HL), was synthesized *via* the reaction of 2-aminophenol with 4-trifluoromethylbenzaldehyde in methanol using a catalytic amount of formic acid. Its corresponding palladium(II) complex, formulated as [PdL_2], was subsequently obtained from the reaction of the HL with $Pd(OAc)_2$ in the presence of sodium acetate. The HL and PdL_2 were characterized by FTIR, UV–Vis, ^{1}H and ^{13}C NMR, CHN elemental analysis, and mass spectrometry. Spectroscopic and analytical data confirmed successful Schiff base formation and bidentate coordination to the Pd(II) center through the azomethine nitrogen and deprotonated phenolic oxygen atoms. the FTIR spectrum of PdL_2 showed a shift of the ν(C=N) and ν(C–O) bands and the appearance of Pd–N and Pd–O vibrations, validating metal-ligand bond formation. UV-Vis data supports a square-planar geometry around a diamagnetic Pd(II) center. TGA revealed enhanced thermal stability, with decomposition occurring above 230 °C and leaving PdO as the final residue. The para-substituted CF_3 moiety is believed to contribute to the rigidity and stability of the coordination framework. In general, the data obtained affirms the successful synthesis of thermally robust, square planar Pd(II) complex derived from trifluoromethyl-substituted Schiff base ligand and contribute to structural chemistry of Pd(II) imine-phenol derivatives. The results of DFT calculations validated the experimental data.

Keywords: Schiff base, Palladium(II) complex, 2-aminophenol, 4-trifluoromethylbenzaldehyde, Square-planar geometry.

Introduction

Schiff bases are among the prominent ligands in the domain of coordination chemistry, owing to their fascinating properties such as tunability, reaction propensity, and affinity toward formation stable complexes with a various metal ions, including transition and main group metals (Boulechfar *et al.,* 2023; Ghanghas *et al.,* 2021). Presence of azomethine moiety (-HC=N) in

Corresponding Author: **Ibrahim Waziri**
Department of Pure and Applied Chemistry, University of Maiduguri, P.M.B. 1069, Maiduguri, Borno State Nigeria
Email: waziriibrahim@unimaid.edu.ng; oo.wahab@nda.edu.ng

©2026 Creative Common License Attribution 4.0 International

Schiff base enables it to easily coordinate with metal ions through the lone pair of electron on the azomethine nitrogen atom, resulting in a strong chelation to the metal center in variety of oxidation states and geometries (Fekri *et al.,* 2019; Rao *et al.,* 2024). In recent times, Schiff bases continues to receive significant attention among coordination chemist not because of their ease synthesis, but for valuable insight they provided into interaction between metal and ligands, nature of their bonding, and structural changes they offers through ligand design (Joshi, 2025; Lv *et al.,* 2025; Waziri, Sookai, *et al.,* 2025).

Within the sphere of different transition metals, palladium occupies a central position due to its ability to form a perfect square planar coordination geometry and stable complexes, especially with N,O-donor ligands (Das *et al.,* 2023; Waziri, Yusuf, *et al.,* 2023). Researches on palladium complexes derived from Schiff bases are of enduring importance toward understanding nature of bonding and electronic interaction between the metal ion and organic ligands (de Oliveira Amaral *et al.,* 2025; Ruiz *et al.,* 2005). Additionally, molecular and spectral characterization of such compounds provides foundation for understanding the reactivity behavior and catalytic potentials, even without practical applications (Ayyannan *et al.,* 2020; Bougossa *et al.,* 2024).

In modern coordination chemistry, substituents are vital in determining structures and properties of Schiff bases (Xiao and Cao, 2020). Notably, the inclusion of electron withdrawing moieties such as trifluoromethyl (-CF_3), can significantly influence the ability of the ligand to donate electron and modulate the coordinating environment spectral character of the resulting complexes (Xiao and Cao, 2018; Zhang *et al.,* 2024). Having this knowledge is important for designing ligands and prediction of metal to ligand interaction. Apart from experimental design for ligands and their complexes, computational study provide complementary information regarding spectral changes and electronic structures (Göktürk *et al.,* 2025).

Herein, a novel Schiff base ligand was prepared through a reaction between 2-aminophenol with 4-(trifluoromethyl)benzaldehyde, and resulting ligand was further reacted with palladium(II) ion using its corresponding acetate salt to a complex. The Schiff base ligand and it palladium complex was subjected various characterization techniques for structural validations, such as fourier transformed infrared, ultraviolet visible, nuclear magnetic resonance, mass spectroscopy and elemental analysis, and rationalized by computational study to further gain insight to coordination behaviors. The structural behaviors of the ligand and its complex was discussed based on the role electron-withdrawing (CF_3) substituent group and the spectral feature that affirm the successful formation of the compounds.

2.0 Materials and Method

Chemicals and Reagents

For this study, following chemical and reagents were used: 2-aminophenol, 4-(trifluoromethyl)benzaldehyde, palladium(II) acetate, methanol, ethanol, dichloromethane, hexane, acetonitrile, toluene, dimethylformamide, dimethyl sulfoxide and acetone. The chemical was obtained from Merck Life Sciences (Pty) Ltd. and was used without any furtherpurifications.

Synthesis of the Schiff base ligand (HL)

To synthesized the Schiff base ligand, condensation reaction protocol was utilized following a modified version of our previously reported methods (Lawan *et al.,* 2024; Waziri, Masena, *et al.,* 2023; Waziri, Yusuf, *et al.,* 2025). Equal amount of aldehyde and the primary amine was used to achieve the condensation reaction. This involve; 4-(trifluoromethyl)benzaldehyde (0.5 g, 0.003 mol, 1.0 equivalent) was dissolved in 20 mL of methanol and stirred using magnetic stirrer at ambient temperature. To the stirring solution of the aldehyde, primary amine, 2-aminophenol (0.31 g, 0.003 mol, 1 equivalent) previously dissolved in 20 mL was added slowly with a continuous stirring. Thereafter, formic acid (three drops) was introduced to the mixture as a catalyst to fast-track the reaction. Thereafter, the mixture was stirred at ambient temperature for 3 h, during which a yellow precipitate gradually formed, signifying the formation of the azomethine (Schiff base) compound. The complete utilization of the carbonyl and amine group was monitored using TLC (hexane/ethyl

acetate; 1:9). After completion, the reaction mixture was allowed to stand for thirty minutes to enhance precipitation. The product was collected by gravity filtration and washed with cold methanol to remove other components which have not reacted and air-dry to afford the Schiff base compound. The dried product was subjected to spectroscopic and analytical characterization for structural confirmation and purity validation, **Scheme 1**.

Yellow powder, yield (0.65 g, 85.44 %), m.p. 146 °C; ^{1}H NMR (500 MHz, DMSO-d_6): □(ppm): 9.14 (s, 1H, OH), 8.38 (s, 1H, HC=N), 8.24 (d, 2H, J = 8.0 Hz, Ar-H; aldehyde-ring), 7.87 (d, 2H, J = 8.0 Hz, Ar-H; aldehyde-ring), 7.27 (d, 1H, J = 7.5 Hz, Ar-H; amine-ring), 7.13 (t, 1H, J = 7.5 Hz, Ar-H; amine-ring), 6.92 (d, 1H, J = 8.0 Hz, Ar-H; amine-ring), 6.86 (t, 1H, J = 7.5 Hz, Ar-H; amine-ring); ^{13}C NMR (125 MHz, DMSO-d_6): □ (ppm): 156.6 (C=N), 150.3 (C-O, Ar-C; amine-ring), 138.9 (CF_3), 136.1, 129.7, 129.4, 128.3, 127.0, 124.5 (aldehyde ring), 124.4(2C), 124.1, 118.4, 118.2, 115.1 (amine ring); UV-Vis: λ(nm): 220 ($\pi\rightarrow\pi^*$), 270 ($\pi\rightarrow\pi^*$), ($n\rightarrow\pi^*$); Elemental Composition (CHN) for $C_{14}H_{10}F_3NO$: Calculated = C, 63.40, H, 3.80, N, 5.28; Experimentally obtained = C, 63.38, H, 3.80, N, 5.26; Molecular weight, *m/z* for $C_{14}H_{10}F_3NO$: Calculated = 266.0812 $[M+H]^+$; Experimentally obtained = 266.0785 $[M+H]^+$.

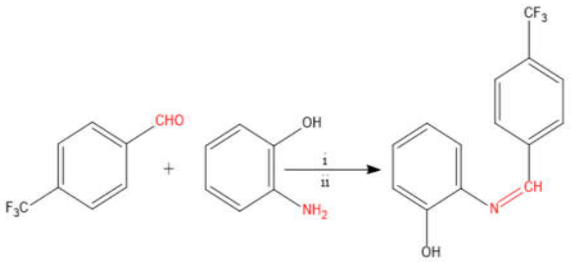

Scheme 1: Illustration of the pathway for the synthesis of the trifluoromethyl-substituted Schiff base ligand (HL); Reagents and conditions: (i) CH_3OH/HCOOH, (ii) = RT/3 hours

Synthesis of the Palladium(II) Complex (PdL_2)

The complex (PdL_2) was prepared using 1:2 mole ratio of palladium(II) acetate to the synthesized ligand using a previously described literature procedure with a slight modification (Waziri, Sookai *et al.,* 2025). In brief, to a methanolic (20 mL) solution of the synthesized ligand HL (0.27 g, 0.001 mol, 2 equivalent) in a 100 mL reaction flask stirring at 65 °C, CH_3COONa (0.11 g, 0.0013 mol, 2.3 equivalent) was added to promote deprotonation of the phenolic (OH) group and facilitate complex formation. The stirring continued for one hour to ensure complete deprotonation. Thereafter, $Pd(OAc)_2$ (0.11 g, 0.0005 mol, 1 equivalent) previously dissolved in 10 mL of methanol was introduced to the reaction mixture *via* a slow addition under continuous string. The reaction was maintained for three hours at 65 °C, during which a dark brown precipitate gradually evolves, signaling chelation between the Pd(II) and HL. After three hours, the reaction was stopped and allowed to cool to ensure maximum precipitation of the product. The precipitate was collected *via* gravity filtration and washed with cold methanol to get rid of the uncoordinated ligand or metal salt, and dry in air. A dark-brown solid product was obtained, and percentage yield was estimated. It was subjected to characterization techniques for structural validation/confirmation, **Scheme 2.**

Dark brown powder, yield (0.21 g, 62.4%), m.p. 283-285 °C (melted); ^{1}H NMR (DMSO-d_6); □(ppm): 8.9 (s, 1H, HC=N, imine), 8.42 (d, 1H, J = 8.0 Hz, Ar-H; aldehyde ring), 8.20 (d, 1H, J = 8.0 Hz, Ar-H; aldehyde ring), 8.13 (d, 1H, J = 8.5 Hz, Ar-H; aldehyde ring), 7.99 (d, 1H, J = 7.5 Hz, Ar-H; aldehyde ring), 7.86 (d, 1H, J = 8.0 Hz, Ar-H; amine-ring), 7.21 (d, 1H, J = 7.5 Hz, Ar-H; amine ring), 7.07 (t, 1H, J = 7.5 Hz, Ar-H; amine ring), 6.96-6.76 (m, 1H, J = 8.0 Hz, Ar-H; amine ring); ^{1}H NMR (125 MHz, DMSO-d_6); □(ppm): 192.5 (C=N, imine), 174.2 (C-O; amine ring), 157.6 (CF_3), 151.8, 150.3, 141.2, 140.1, 137.2, (aldehyde-ring); 129.1, 125.6, 125.4, 118.8, 116.4, 111.1 (amine-ring); $FTIR_{ATR}$: U(cm^{-1}): 1581 (C=N), 1465 (C-N), 1311 (CF_3), 833 (C-H), 501 (Pd-O), 401 (Pd-N); UV-Vis: λ(nm): 235 ($\pi\rightarrow\pi^*$), 295 ($\pi\rightarrow\pi^*$), 435 (LMCT); Elemental Composition (CHN) for $C_{28}H_{18}F_6N_2O_2Pd$: Calculated = C, 52.97, H, 2.86, N, 4.40; Experimentally obtained = C, 52.93, H, 2.84, N, 4.40; Molecular weight, *m/z* for $C_{28}H_{18}F_6N_2O_2Pd$: Calculated = 634.0312 $[M]^+$; Experimentally obtained = 633.5455 $[M]^+$

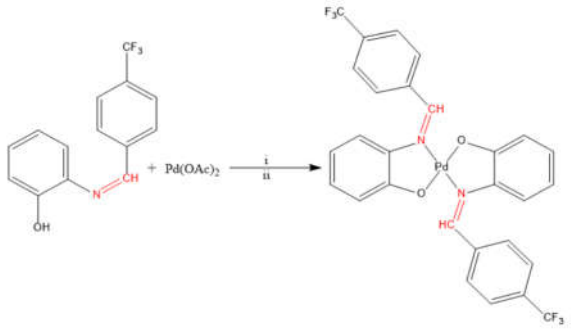

Scheme 2: Illustration of the pathway for the synthesis of the trifluoromethyl-substituted Schiff base derived palladium(II) complex (PdL_2); Reagents and conditions: (i) = CH_3OH/CH_3COONa, (ii) = 65 °C/4 hours.

Measurements and Instrumentation

To validate and confirm the molecular structures of the compounds, spectroscopic techniques were deployed using the following instruments: proton and carbon spectra were recorded on a 500 MHz, Bruker Avance spectrometer, utilizing solvent DMSO-d_6 at ambient temperature. The functional group validation was accomplished using solid samples on Perkin-Elmer BX, FT-IR spectrometer (Bruker Tensor 27), within the wave number range of 4000-400 cm^{-1} at room temperature. The Electronic spectra were obtained on a Perkin-Elmer UV-V-s spectrophotometer within wavelength range of 200-800 nm at room temperature using sample concentration of 10^{-3} M in dimethyl sulfoxide. For the stoichiometric composition, elemental (CHN) analysis was performed on a Vario EL III Elementar microanalyzer to estimate the compositions of carbon, hydrogen, and nitrogen in the compounds. Molecular weight of compounds was validated using a Waters Acquity UPLC Synapt G2 HD mass spectrometer.

Density Functional Theory (DFT) Study

Following the confirmation of the structures of HL and PdL_2 based on the spectroscopic characterization data obtained. The compounds were subjected to quantum chemical investigation to explore their molecular and electronic properties. Geometry optimizations together with frequency calculations were carried out on the well prepared input structures of the synthesized compounds, allowing them to relax to their respective equilibrium (global minimum) geometries using the B3LYP functional (Becke, 1992; Lee *et al.,* 1988) combined with the Def2TZVP basis set (Weigend, 2006; Weigend and Ahlrichs, 2005). This function and basis set were selected because they have been validated for transition metal complexes and are known to provide accurate data, and electronic description for metal ions and their ligands at low computational cost. To prepare the structures of the compounds, the GaussView 5.0 interface (Dennington *et al.,* 2009) was used, and the DFT calculations were performed using the Gaussian 09 program (Frisch, *et al.,* 2009), achieving compliance with standard optimization protocol.
HOMO and LUMO energy values of the optimized species were used to calculate global reactivity parameters using Equations 1-3 (Wahab *et al.,* 2018, 2020), and electrostatic potential maps were utilized to deduce susceptibility to nucleophilic or electrophilic attack. Lastly, stability and strength of the metal to ligand interactions were evaluated *via* natural bond orbital (NBO) analysis based on second-order perturbation theory.

$$\text{Energy gap } (E_g) = E_{LUMO} - E_{HOMO} \quad (1)$$

$$\text{Global softness } (S) = \frac{2}{E_g} = \frac{2}{E_{LUMO} - E_{HOMO}} \quad (2)$$

$$\text{Electronegativity } (\chi) = -\frac{1}{2}(E_{LUMO} + E_{HOMO}) \quad (3)$$

3.0 Results and Discussion

Chemistry

The trifluoromethyl-substituted Schiff base ligand (HL) was obtained through an equimolar condensation reaction between 2-aminophenol (primary amine) with 4-(trifluoromethyl)benzaldehyde (aldehyde) in alcoholic medium (methanol) in the presence of mild acidic condition (formic acid) to aid in facilitating the reaction. The reaction was performed at ambient temperature, affording the ligand as a brown crystalline solid within three hours of stirring. The formation of the imine (CH=N) moiety was indicated by the evolution of colour in the reaction mixture and further validated by characterization techniques detailed in the subsequent sections. The synthetic route is illustrated in **Scheme 1**.

The corresponding palladium(II) complex, coded as [PdL_2], was obtained through a ligand-to-metal reaction involving two mole equivalents of the Schiff base and Pd(II) ion (one equivalent) utilizing palladium(II) acetate as the source of the ion in methanolic medium, in the presence of CH_3COONa as a base. The use of sodium acetate promoted deprotonation of the phenolic proton, facilitating chelation of HL to the palladium center through the nitrogen and oxygen atoms of imine and hydroxyl moieties. The reaction was conducted under reflux at 65 °C for three hours, leading to the formation of a dark brown solid product, which was isolated, washed, and dried to yield the target complex. The pathway leading to the complexation reaction is illustrated in **Scheme 2**.

The HL and PdL_2 were non-sensitive to air and moisture and are solid in nature. They were found to be soluble in dimethyl sulfoxide, dimethyl formamide, and methyl cyanide, but insoluble non-polar solvents like hexane and toluene. The formation and purity of the compounds were confirmed through standard spectroscopic and analytical techniques. On the basis these characterization techniques, the data obtained corroborated well with the expected molecular and stoichiometric composition of HL and PdL_2.

Spectroscopic Characterization

NMR Spectroscopy

The spectra of the ligand and its complex was recorded in DMSO-d_6 to confirm the mode of coordination and the formation of the azomethine linkage. The proton spectrum of HL (Figure 1A) shows the characteristic imine proton (-CH=N-) as a sharp singlet at δ ~8.38 ppm, confirming imine formation (Saritha and Metilda, 2021). Aromatic signals appear in the region δ 6.86–8.24 ppm, including two well-defined doublets integrating to 2H each, arising from the AA′BB′ symmetry of the *p-CF₃* substituted benzene ring. A broad downfield resonance corresponding to the hydroxyl moiety is observed at 9.14 ppm, consistent with hydrogen-bonded hydroxyl functionality (Kumar *et al.,* 2024; Rana *et al.,* 2025).

Upon coordination to Pd(II), the spectrum of PdL_2 (Figure 1B) shows three key changes. First, the phenolic (-OH) signal disappears, confirming deprotonation and O-coordination to Pd(II). Second, the imine proton shifts downfield (δ 8.88 ppm) as the result of deshielding upon N-chelation. Third, the former 2H aromatic doublets split into 1H signals, indicating loss of magnetic equivalence within the aromatic ring system. This splitting is consistent with loss of symmetry after coordination and strongly supports the presence of two inequivalent ligand environments, which is characteristic of a cis-square-planar Pd(II) geometry (Kumar *et al.,* 2024).

The carbon spectrum data support the observations from the proton spectra. In the ligand (Figure 2A), the imine carbon (C=N) resonates at δ ~156 ppm, while aromatic carbons appear within δ 115–150 ppm, consistent with the proposed salicylidene structure. In the Pd(II) complex (Figure 2B), the azomethine carbon shifts slightly downfield, again reflecting coordination of the imine nitrogen. The aromatic carbons display systematic downfield shifts, particularly those ortho to the metal-binding sites, due to the electron-withdrawing effect of the Pd(II) center (Chen *et al.,* 2019). The summary of the comparative ^1H and ^{13}C NMR is provided in Table 1.

Overall, the combined proton and carbon NMR data confirm successful formation of the Schiff base and its subsequent chelation to Pd(II) through the *O,N*-donor set, accompanied by loss of symmetry and increased deshielding, fully consistent with the proposed cis-[PdL_2] square-planar structure.

Table 1: Summary of ^1H and ^{13}C NMR Spectral Data

Compounds	Proton signals (ppm)			Carbon signals (ppm)			
	OH	HC=N	Ar-H	C=N	C-O	Ar-C	CF_3
HL	9.14	8.38	8.24-6.86	156.6	150.3	138.9	136.1-115.1
PdL_2	-	8.88	8.42-6.81	192.5	174.2	157-111.1	137.1

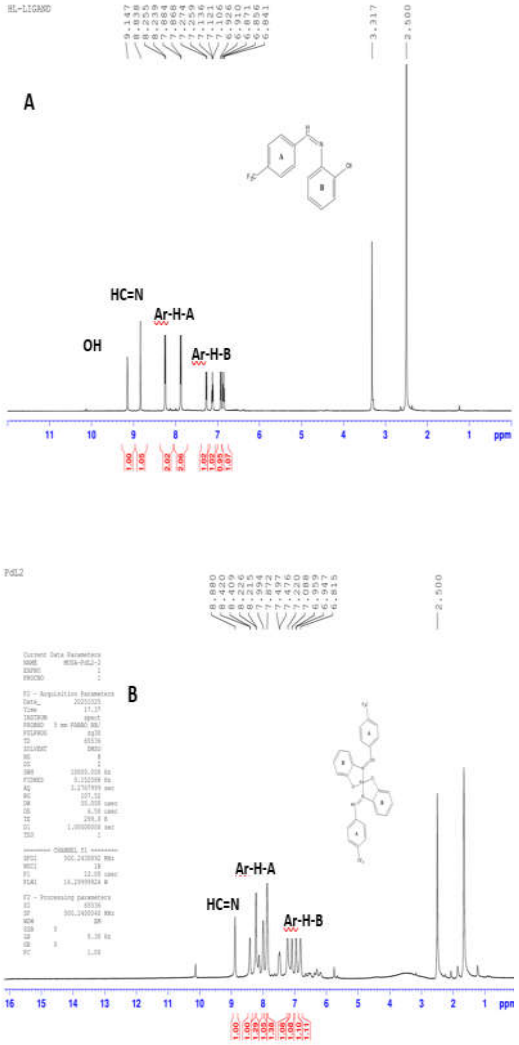

Figure 1: ^{1}H NMR spectra of (A) the ligand (HL) and (B) its complex (PdL_2), recorded in DMSO-d_6 at 500 MHz.

FTIR Spectroscopy

The FT-IR spectra of (HL) (Figure 3A) and PdL_2 (Figure 3B) display diagnostic differences that support coordination through nitrogen and oxygen atoms of imine and phenolate moieties. In the ligand spectrum (Figure 3A), a band at 3332 cm^{-1} is assigned to the O-H stretching vibration, and a strong band at 1627 cm^{-1} corresponds to the ν(C=N) stretching vibration (Bano *et al.,* 2025). In the spectrum of the complex (Figure 3B) the broad O-H band is absent, consistent with the disappearance of the phenolic proton on coordination. Concomitantly, imine band is shifted to 1581 cm^{-1} (Δ ≈ 46 cm^{-1} to lower wavenumber), indicating deshielding/weakening of the C=N bond because of electron donation from the imine nitrogen to the Pd(II) centre.

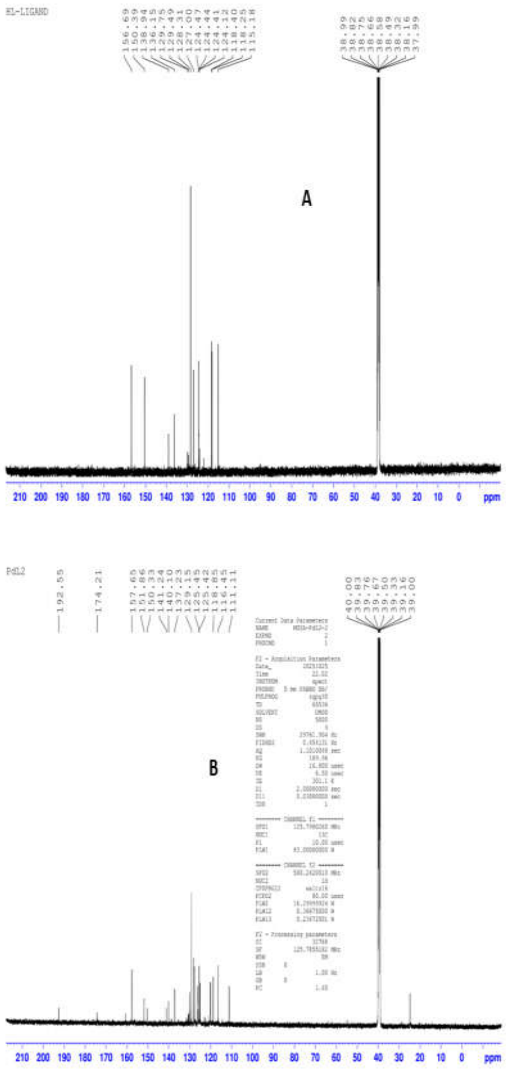

Figure 2: ^{13}C NMR spectra of (A) the ligand (HL) and (B) its complex (PdL_2), recorded in DMSO-d_6 at 125 MHz.

Vibrations attributed to the trifluoromethyl substituent $\nu(C\text{-}F)_{asy}$ at ~1319 cm^{-1} and $\nu(C\text{-}F)_{sy}$ at ~1110 cm^{-1} in the ligand, remain present in the complex with small shifts (1319 →1311 cm^{-1}; 1110 →1064 cm^{-1}), showing that the CF_3 group is preserved but that its local electronic environment is modestly perturbed by coordination. Importantly, new weak-to-moderate bands appear

in the low-frequency region of the complex spectrum (notably: 594, 501 and 401 cm^{-1}) and can be assigned to metal–ligand vibrations (ν(Pd-O) and ν(Pd-N)) and other Pd-ligand lattice modes. The retention of aromatic C-H out-of-plane bending patterns (≈ 830, 748 cm^{-1}) also indicates that the substitution pattern of the aromatic rings is unchanged upon complex formation (Elsayed *et al.,* 2024).

Taken together, the disappearance of the phenolic O-H band, the substantial downshift of the ν(C=N) band, the appearance of new Pd-N/Pd-O bands, and the modest shifts in CF_3-related vibrations provide strong spectroscopic evidence that HL binds to palladium in a bidentate N,O-fashion, yielding the neutral [PdL_2] complex proposed in **Scheme 2**.

A comparative bar chart (Figure 4) illustrating the characteristic vibrational shifts before and after complexation clearly shows the disappearance of the O–H band in PdL_2, alongside a downward shift in the C=N and C–O stretching frequencies, confirming the coordination of the azomethine nitrogen and phenolic oxygen atoms to the Pd(II) ion.

UV-Visible Spectroscopy

The electronic spectra of HL and PdL_2 were recorded in DMSO solution to investigate the electronic transitions and the geometry around the palladium center. The UV–Vis spectrum of HL (Figure 5A) exhibited two intense bands at 220 and 270 nm assigned to π→π* transitions of the aromatic and azomethine chromophores, alongside a weaker n→π* transition at 350 nm associated with the lone pair on the imine nitrogen (Sarto *et al.,* 2020). Upon complexation with Pd(II), leading to the formation of PdL_2 these bands shifted to 235 and 295 nm, and the n→π* band at 350 nm disappeared, giving rise to a new broad absorption at 435 nm attributable to ligand-to-metal charge transfer (LMCT)/d→d transitions (Figure 5B) (Elsayed *et al.,* 2024). The broadening of the absorption band in visible region is due to Laporte-forbidden d→d transitions typical of metal ions with d^8 configuration. The appearance of bathochromic shifts demonstrates enhanced conjugation and increased rigidity of the coordination framework, affirming chelation through *O,N*-donor atoms. In addition, the estimated energies of transition calculated from $E = \frac{1240}{\lambda}$ (Table 2) revealed a consistent decrease upon complexation, showcasing the stabilization of the excited states within the complex compound. This trend of this feature is virtually illustrated in the form of bar chart (Figure 6), which demonstrated the reduced transition energies for absorption bands in PdL_2 compared to the free HL. Collectively, these observations affirm a rigid interaction between the palladium ion and HL, and the development of an d→d/LMCT pathway in the complex (Bagheri *et al.,* 2024).

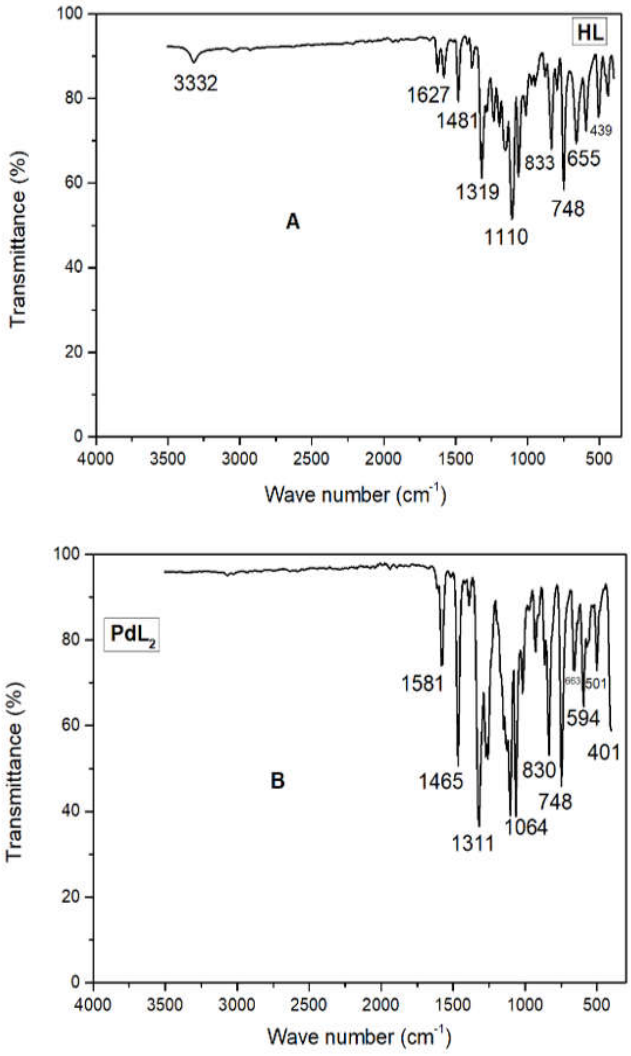

Figure 3. FT-IR spectra of (A) the ligand (HL) and (B) its complex (PdL_2) at recorded room temperature using ATR method in solid state.

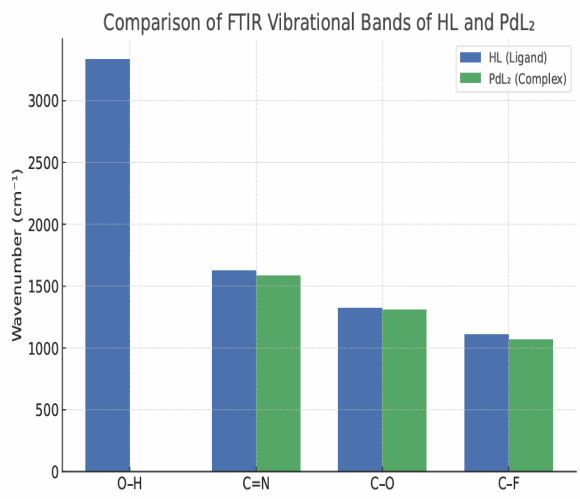

Figure 4: Comparative bar chart illustrating the shifts in selected FTIR vibrational bands in spectra the ligand (HL) and its complex (PdL_2).

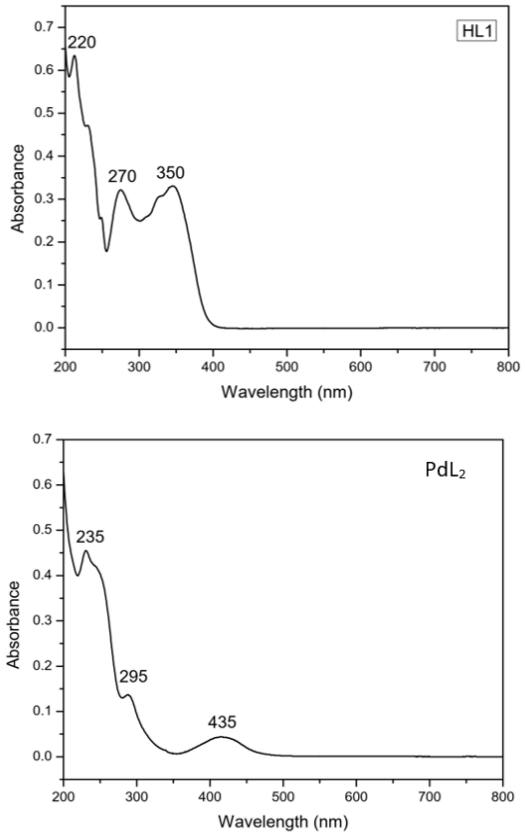

Figure 5: Electronic absorption spectra of (A) the ligand (HL) and (B) its complex (PdL_2), showing the wavelength of absorption of the compounds.

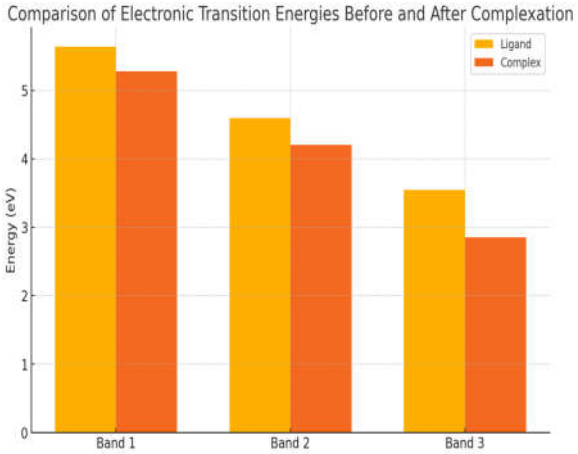

Figure 6: Bar chart comparing the electronic transition energies of HL and its Pd(II) complex PdL_2, showing reduced transition energies after complexation.

Mass Spectrometry

To further complement the other characterization, obtain and validate the structures of compounds, mass spectral analysis was performed. The spectral shows prominent peak with *m/z* values at 266.0785 and 633.5455, corresponding to $[M+H]^+$ and $[M]^+$ for HL and PdL_2. These values correlate well with calculated molecular weight of 266.0812 and 634.0312 g/mol for the HL and PdL_2. Furthermore, appearance of isotopic typical of palladium on the spectrum of the complex further validates the presence of metal center. Fragmentation patterns that indicate loss of a ligand unit and other smaller fragments were noted on the spectra of the complex, which confirms the proposed molecular composition and stability of the complex.

Thermal Analysis (TGA/DTG)

The Thermal behavior of HL and PL_2 was evaluated using thermogravimetric analysis within the temperature region of 25-800 °C (Figure 7A-B). Thermogram of HL (Figure 7A) presented a single major decomposition step from 145 to 380 °C, which accounted for 95-96% weight loss. The lack of any other decomposition step below 150 °C on the thermogram shows that the ligand does not contain moisture or lattice solvent, and reflect direct decomposition of organic units, with approximately 4% residual mass associated with carbonaceous residue.

Table 2: Comparison of λmax and electronic transition energies before and after complexation

Band	λmax (Ligand) (nm)	Energy (Ligand) (eV)	λmax (Complex) (nm)	Energy (Complex) (eV)	Assignment
1	220	5.64	235	5.28	π→π* (Aromatic ring)
2	270	4.59	295	4.20	π→π* (Ring–C=N conjugation)
3	350	3.54	435	2.85	n→π* (Ligand) → LMCT (Complex)

6158

Conversely, the thermogram of PdL_2 displays multiple decomposition steps that show enhanced structural rigidity and unveiling the presence of metal ion. The first decomposition step within 200 °C with a weight loss of 19.4% is attributed to detachment or decomposition of weakly bound fragments from the partial degradation of the ligand. The second decomposition step which occurs within the temperature range of 200-300 °C, with 34.1 % weight is attributed to the progressive breakdown of the Schiff base backbone. While the third decomposition step within the temperature range of 300-400 °C, and a weight loss of 32 % is due to the final decomposition of the coordinated ligand fragments. A steady and stable curve on the thermogram at above 450 °C is associated with the formation of thermally stable metal oxide (PdO/Pd-containing inorganic residue). This is typical of square planar Pd(II) complexes.

Comparing the two thermograms, the profile of PdL_2 shows greater thermal stability than the free Schiff base ligand. This is evidence by (a) the slow onset of major decomposition, (b) multi-steps decomposition which is due to the metal ion stabilization of the ligand framework, (Rappé *et al*., 1992), and coupled with presence of inorganic residue. This further indicates that coordination enhances the rigidity of the ligand system, common observation in complexes with d^8 metal center. In addition, -I effect of para-substituted trifluoromethyl moiety stiffens the ligand-complex and delays thermal scission.

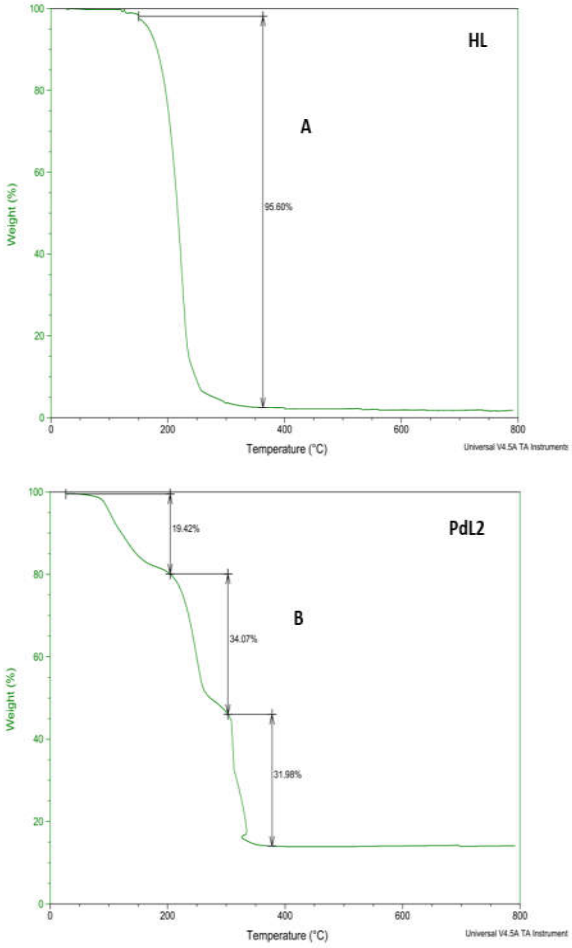

Figure 7: The thermogram of (A) the ligand (HL) and (B) its complex (PdL_2) showing the decomposition steps as a function of increased temperature.

Proposed Structure

Based on the combined spectroscopic (FTIR, NMR, UV-Vis, and Mass), TGA, and analytical data, the ligand (HL) coordinates to the Pd(II) ion through the azomethine nitrogen and deprotonated phenolic oxygen donor sites. The

1:2 metal-to-ligand stoichiometry was supported by CHN elemental analysis, and mass spectral data, confirming the formulation as [PdL_2]. The proposed structure of the complex is depicted in Scheme 2, showing a square-planar geometry with two bidentate Schiff base ligands arranged around the Pd(II) center. The diamagnetic nature of the complex, and the characteristic MLCT absorption band in the visible region further support this geometry. Additionally, the presence of the strong electron-withdrawing CF_3 substituent enhances structural rigidity and promotes better electron delocalization across the ligand framework, which assists in stabilizing the square-planar arrangement. This substituent effect, coupled with observed multistep thermal behavior, suggests that the CF_3 group contributes to the overall thermodynamic stability of the Pd(II) complex.

Density Functional Theory (DFT) Study

Structural Analyzing of the optimized compounds

Table 3 shows the optimized structures of HL and PdL_2, frontier molecular orbital (HOMO and LUMO) isosurfaces, and their electrostatic potential maps (ESP). Two molecules of the Schiff base (the deprotonated form) are coordinated to the Pd(II) ion, forming a stable and symmetric square planar geometry, where the donor atoms (nitrogen and oxygen) are oriented in a *trans* manner. The Schiff base interacted with the metal ion as an anionic ligand, resulting in a neutral complex whose geometry is consistent with the experimental proposition as evidenced by key geometrical descriptors (bond lengths and bond angles) listed in Table 4.

Table 3: Optimized geometries, frontier molecular orbital isosurfaces, and electrostatic potential maps of the ligand (HL) and the complexes (PdL_2).

	HL	PdL_2
Optimized geometry	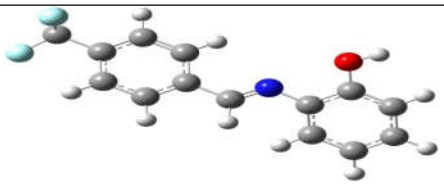	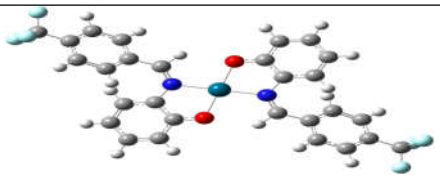
HOMO isosurfaces	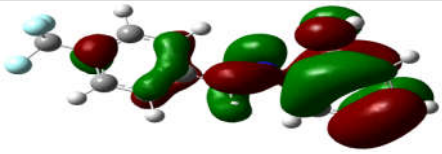	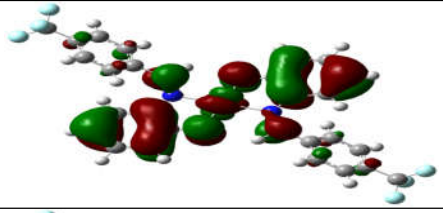
LUMO isosurfaces	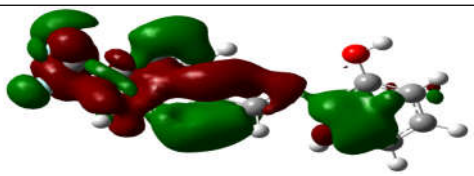	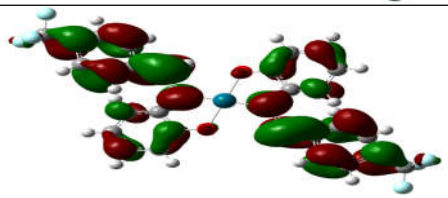
ESP map	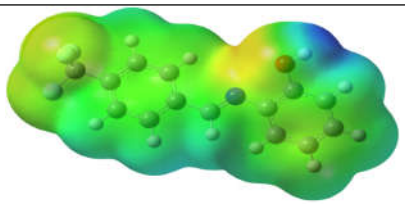	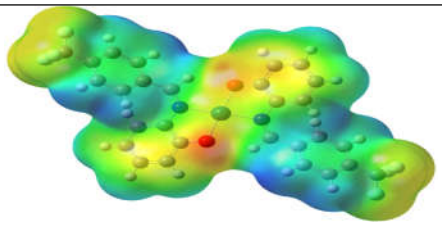

Table 4: Comparison of geometrical and reactivity descriptors between HL and PdL_2.

Geometrical descriptors	HL	PdL_2	Reactivity descriptors	HL	PdL_2
C – O (Å)	1.36	1.31	**E_{HOMO} (eV)**	-6.13	-5.59
C = N (Å)	1.27	1.29	**E_{LUMO} (eV)**	-2.25	-2.84
Pd – O (Å)	-	2.00	**E_g (eV)**	3.88	2.75
Pd – N (Å)	-	2.04	**S (eV)**	0.51	0.72
∠O-Pd-O (^{O})	-	180.00	**χ (eV)**	4.19	4.22
∠N-Pd-N (^{O})	-	180.00	-	-	-
∠N4-Pd-O3 (^{O})	-	97.49	-	-	-
∠N4-Pd-O2 (^{O})	-	82.50	-	-	-

The coordination of HL to Pd(II) ion is accompanied by shortening/strengthening of the C–O bond with elongation of the C-N bond, marking a change in electron density in these bonds upon coordination. The changes in C–O and C–N bond lengths between the ligands and the complexes are attestations to the occurrence of coordination. Similarly, the appearance of bands for metal-ligand bonds in the fingerprint region (Figure 3) is also justified by the relatively long Pd–O and Pd–N bonds (≥2.00 Å) (Table 4). As expected of a perfect square planar geometry, the angles between opposite vertices i.e., ∠O-Pd-O and ∠N-Pd-N in the complex are linear (180 ^{O}), whereas those of the perpendicular vertices i.e. $\angle N_4$-Pd-O_3 and $\angle N_4$-Pd-O_2 are around 90 ^{O}, with their sum equating to 180 ^{O}.

Quantum Reactivity Analysis

The HOMO isosurfaces represent the molecular orbitals from which electrons can be withdrawn by an electrophile during an interaction. In the studied compounds, these isosurfaces are predominantly localized over the delocalized π-ring systems, but to a lower extent in the phenyl ring bearing the CF_3 substituent, signaling the electron-depleting influence of this substituent. Conversely, LUMO isosurfaces identify the molecular orbitals into which electrons can be introduced by a nucleophilic species. These are generally distributed across the entire molecular framework except for the metal center in the complex which suggests that the d-orbitals are saturated by electron donation from the ligand.

From a quantum-chemical standpoint, the electron-donating and electron-accepting tendencies of molecules can be inferred quantitatively from their HOMO and LUMO energies. Molecules with higher (less negative) E_{HOMO} values can donate electrons more readily, while molecules with lower (more negative) E_{LUMO} values possess enhanced electron-accepting ability. Based on the E_{HOMO} and E_{LUMO} values listed in Table 4, the metal complexes display improved electron-donating and/or electron-accepting characteristics relative to the free ligand, reflecting the influence of metal coordination on the electronic structure.

The energy gap (E_g) and softness (S) are key quantum reactivity descriptors used to assess molecular susceptibility to changes in electron density or electronic configuration. A smaller E_g indicates a softer molecule, higher excitability, lower resistance to electron density perturbation, and consequently, higher chemical reactivity. Following the trend in E_g (Table 4), the complex is predicted to be more reactive than the ligand, which aligns with the antimicrobial activity trend discussed earlier. The enhanced activity of the complex relative to the ligand is attributable to its amphoteric (electron-donating and electron-withdrawing) nature as suggested by its E_{HOMO} and E_{LUMO}.

Electronegativity (χ), which signifies the electron-pulling power of a species, follows the order: PdL_2 > HL, indicating the superior oxidizing ability of the complex compared to the ligand.

Molecular Electrostatic Potential Map

The electrostatic potential maps (ESP) in Table 3 illustrate the electron density distribution throughout the compounds. Electron-rich and

electron-deficient regions are distinguished by color: red indicates the highest electron density, blue the lowest, and orange and yellow represent moderately and weakly dense areas, respectively. Green denotes regions of near-zero potential (Fugu *et al.,* 2025). These color patterns reveal that electron density is concentrated around donor heteroatoms, supporting their role as preferred coordination sites. The red regions in the complexes correspond closely with the HOMO isosurface distribution. Yellow regions in the complexes indicate areas susceptible to weak electrophilic attack, capable of participating in hydrophobic interactions in biological systems, and likely to engage in π–π stacking which is useful for crystal packing.

NBO analysis of metal-ligand bond strength

The strengths of metal–ligand (Pd-O and Pd-N) bonds were assessed quantitatively based on stabilization energy E(2) derived from second-order perturbation theory treatment of Natural Bond Orbitals (NBO) (Wahab *et al.,* 2025). Higher E(2) values indicate stronger donor–acceptor interactions and greater bond stability. The E(2) values in Table 5 show that the ligand forms stable Pd-O and Pd-N bonds with Pd^{2+} through its N- and O-donor atoms, respectively. However, the O-donor bond (Pd-O) with stabilization energy of 81.92 kcal/mol is stronger than the N-donor (Pd-N) bond with 78.34 kcal/mol stabilization energy. This is likely due to the higher electronegativity of oxygen.

Table 5: Stabilization energies of PdL_2 as obtained from second order perturbation analysis of NBO basis.

Complex	Donor NBO (i)	Acceptor NBO (j)	E_j-E_i (kcal/mol)	$F_{i,j}$ (kcal/mol)	E(2) (kcal/mol)
Complex **1**	LP(O)	LP*(Pd)	0.18	0.13	81.92
	LP(N)	LP*(Pd)	0.16	0.12	78.34

5.0 Conclusion

In this study, a new Schiff base ligand was synthesized via the condensation of 2-aminophenol and 4-trifluoromethylbenzaldehyde under mild conditions, followed by the preparation of its corresponding Pd(II) complex using palladium(II) acetate. Spectroscopic and analytical investigations confirmed the bidentate coordination of the ligand through the azomethine nitrogen and deprotonated phenolic oxygen atoms, resulting in the formation of a neutral square-planar **[**PdL_2] complex. The combined FTIR, NMR, and UV–Vis data validated the proposed coordination mode, while CHN analysis, and TGA supported the purity, stoichiometry, and enhanced thermal stability of the complex. The diamagnetic nature of the complex is consistent with a square-planar geometry typical of Pd(II) systems. Notably, the electron-withdrawing CF_3 substituent contributed to increased ligand rigidity and stabilization of the coordination framework, reinforcing the robustness of the resulting complex. DFT based electronic structure calculations did not only confirm the formation of a perfect square planar geometry with strong/stable metal-ligand bonds but also revealed changes in band gaps and quantum chemical reactivity upon coordination.

Conflict of Interest

The underlisted authors hereby affirm they don't have any computing personal or financial interest that could influence the work reported in this manuscript.

Q2 References

Ayyannan, G., Mohanraj, M., Gopiraman, M., Uthayamalar, R., Raja, G., Bhuvanesh, N., Nandhakumar, R., and Jayabalakrishnan, C. (2020). New Palladium (II) complexes with ONO chelated hydrazone ligand: Synthesis, characterization, DNA/BSA interaction, antioxidant and cytotoxicity. *Inorganica Chimica Acta*, *512*, 119868.

Bagheri, Z., Ghorbanloo, M., Bikas, R., and Lis, T. (2024). Palladium (II) complexes comprising thiazole-hydrazone Schiff base ligand: Synthesis, structure and catalytic activity in Suzuki-Miyaura coupling reactions. *Polyhedron*, *264*, 117245.

Bano, S., Arshi, F., Firdaus, S., Kushwaha, N. K., Singh, S. K., Kumar, A., and Singh, A. K. (2025). Exploring Schiff base and its Palladium complexes: Synthesis, Characterization, Antimycobacterial activity, DFT, Molecular docking and ADME studies. *Journal of Molecular Structure*, 143704.

Becke, A. D. (1992). Density-functional thermochemistry. I. The effect of the exchange-only gradient correction. *The Journal of chemical physics*, *96*(3), 2155-2160.

Bougossa, S., Mhadhbi, N., Ahmed, A. B., Hamdi, M., Elghniji, K., Erwann, J., Hamden, K., Oueslati, A., and Naïli, H. (2024). Design of a new palladium (II) halide complex as a bio-active material: synthesis, physico-chemical studies, DFT-computations and evaluation of anti-inflammatory, antioxidant and anti-gastric damage activities. *RSC Advances*, *14*(25), 17413-17433.

Boulechfar, C., Ferkous, H., Delimi, A., Djedouani, A., Kahlouche, A., Boublia, A., Darwish, A. S., Lemaoui, T., Verma, R., and Benguerba, Y. (2023). Schiff bases and their metal Complexes: A review on the history, synthesis, and applications. *Inorganic Chemistry Communications*, *150*, 110451.

Chen, B., Holstein, J. J., Horiuchi, S., Hiller, W. G., and Clever, G. H. (2019). Pd (II) coordination sphere engineering: pyridine cages, quinoline bowls, and heteroleptic pills binding one or two fullerenes. *Journal of the American Chemical Society*, *141*(22), 8907-8913.

Das, A., Saha, M., Mandal, S., Das, S., Saha, K. D., and Mondal, T. K. (2023). New palladium (II) and platinum (II) complexes with an ONS donor azo-thioether pincer ligand: synthesis, characterization, protein binding study and in vitro cytotoxicity. *New Journal of Chemistry*, *47*(10), 4931-4943.

de Oliveira Amaral, L., Santiago, L. R., Ferreira, W. V., da Silva, J. D. S., Bortoluzzi, A. J., Marques, M. B., Costa, M. J. F., Sette-de-Souza, P. H., and Soares, S. M. (2025). Novel palladium (II) complexes with Schiff bases derived from 4, 5-methylenedioxy-2-nitrobenzaldehyde and 5-Bromo-2-hydroxybenzaldehyde as potential antimicrobial agents: Synthesis, characterization and studies in vitro. *Journal of Molecular Structure*, *1328*, 141403.

Dennington, R., Keith, T., Millam, J., and GaussView, V. (2009). Semichem Inc. *Shawnee Mission KS, GaussView, Version*, *5*(8).

Elsayed, S. A., Elnabky, I. M., Aboelnga, M. M., and El-Hendawy, A. M. (2024). Palladium (II), platinum (II), and silver (I) complexes with 3-acetylcoumarin benzoylhydrazone Schiff base: Synthesis, characterization, biomolecular interactions, cytotoxic activity, and computational studies. *RSC Advances*, *14*(27), 19512-19527.

Fekri, R., Salehi, M., Asadi, A., and Kubicki, M. (2019). Synthesis, characterization, anticancer and antibacterial evaluation of Schiff base ligands derived from hydrazone and their transition metal complexes. *Inorganica Chimica Acta*, *484*, 245-254.

Fugu, M. B., Wahab, O. O., Ndahi, N. P., Mala, G. A., Abd El-Maksoud, M. S., and Waziri, I. (2025). Synthesis, Characterization, Antimicrobial Evaluation, DFT and Molecular Docking Study of Some Transition Metal Complexes Derived From N, N'-(ethane-1, 2-diyl) dipicolinate Ligand. *Journal of Molecular Structure*, 144789.

Ghanghas, P., Choudhary, A., Kumar, D., and Poonia, K. (2021). Coordination metal

complexes with Schiff bases: Useful pharmacophores with comprehensive biological applications. *Inorganic Chemistry Communications*, *130*, 108710.

Göktürk, T., Güp, R., Zengin, T., Hökelek, T., Aksu, E. N., Öztürk, F. S., Toraman, M., Durak, O., Taş, S., and Sakallı Çetin, E. (2025). Effects of electron donating and withdrawing substituents on crystal structures, cytotoxicity and in silico DNA interactions of isatinoxime Schiff base ligands. *Research on Chemical Intermediates*, *51*(1), 433-457.

Joshi, R. (2025). Advancement on the Chemistry of Organotin-Schiff Base Complexes: A Crystallographic Perspective. *Dalton transactions*.

Kumar, M., Singh, A. K., Singh, V. K., Yadav, R. K., Singh, A. P., and Singh, S. (2024). Recent developments in the biological activities of 3d-metal complexes with salicylaldehyde-based N, O-donor Schiff base ligands. *Coordination Chemistry Reviews*, *505*, 215663.

Lawan, S. Y., Mshelia, M. B., Mala, G. A., Olaide, W. O., Musa, S. A., Ahmed, A. A., Yesufu, H. B., and Waziri, I. (2024). Antioxidant Activity and DFT Calculations of Metal Complexes Derived from a Schiff Base Ligand: Synthesis, Characterization, and Biological Evaluation. *ChemistrySelect*, *9*(13), e202400676.

Lee, C., Yang, W., and Parr, R. G. (1988). Development of the Colle-Salvetti correlation-energy formula into a functional of the electron density. *Physical review b*, *37*(2), 785.

Lv, L., Zheng, T., Tang, L., Wang, Z., and Liu, W. (2025). Recent advances of Schiff base metal complexes as potential anticancer agents. *Coordination Chemistry Reviews*, *525*, 216327.

M. J. Frisch, G. W. Trucks, H. B. Schlegel, G. E. Scuseria, M. A. Robb, J. R. Cheeseman, G. Scalmani, V. Barone, B. Mennucci, G. A. Petersson, H. Nakatsuji, M. Caricato, X. Li, H. P. Hratchian, A. F. Izmaylov, J. Bloino, G. Zheng, J. L. Sonnenberg, M. Hada, M. Ehara, K. Toyota, R. Fukuda, J. Hasegawa, M. Ishida, T. Nakajima, Y. Honda, O. Kitao, H. Nakai, T. Vreven, J. A. Montgomery, Jr., J. E. Peralta, F. Ogliaro, M. Bearpark, J. J. Heyd, E. Brothers, K. N. Kudin, V. N. Staroverov, R. Kobayashi, J. Normand, K. Raghavachari, A. Rendell, J. C. Burant, S. S. Iyengar, J. Tomasi, M. Cossi, N. Rega, J. M. Millam, M. Klene, J. E. Knox, J. B. Cross, V. Bakken, C. Adamo, J. Jaramillo, R. Gomperts, R. E. Stratmann, O. Yazyev, A. J. Austin, R. Cammi, C. Pomelli, J. W. Ochterski, R. L. Martin, K. Morokuma, V. G. Zakrzewski, G. A. Voth, P. Salvador, J. J. Dannenberg, S. Dapprich, A. D. Daniels, Ö. Farkas, J. B. Foresman, J. V. Ortiz, J. Cioslowski, and D. J. Fox, Gaussian 09 (Gaussian, Inc., Wallingford CT, 2009).

Rana, M. S., Rayhan, N. M. A., Emad, A. H., Hossain, M. I., Shah, M. M., Kudrat–E-Zahan, M., Hossen, M. F., and Asraf, M. A. (2025). Salicylaldehyde-based Schiff bases and their transition metal complexes: an overview on synthesis and biological activities. *Journal of Coordination Chemistry*, *78*(9), 937-1006.

Rao, D. P., Gautam, A. K., Verma, A., and Gautam, Y. (2024). Schiff bases and their possible therapeutic applications: A review. *Results in Chemistry*, 101941.

Rappé, A. K., Casewit, C. J., Colwell, K., Goddard III, W. A., and Skiff, W. M. (1992). UFF, a full periodic table force field for molecular mechanics and molecular dynamics simulations. *Journal of the American Chemical Society*, *114*(25), 10024-10035.

Ruiz, J., Cutillas, N., Vicente, C., Villa, M. D., López, G., Lorenzo, J., Avilés, F. X., Moreno, V., and Bautista, D. (2005). New palladium (II) and platinum (II) complexes with the model nucleobase 1-methylcytosine: antitumor activity and interactions with DNA. *Inorganic Chemistry*, *44*(21), 7365-7376.

Saritha, T., and Metilda, P. (2021). Synthesis, spectroscopic characterization and biological applications of some novel Schiff base transition metal (II) complexes derived from curcumin moiety. *Journal of Saudi chemical society*, *25*(6), 101245.

Sarto, L. E., Badaró, W. P. D., de Gois, E. P., Barbosa, M. I. F., Torres, C., Viana, R. B., Honorato, J., Castellano, E. E., and de Almeida, E. T. (2020). Crystal structures and DFT analysis of Palladium (II) complexes with Schiff bases derived from N, N-dialkyl-p-phenylenediamines. *Journal of Molecular Structure*, *1204*, 127549.

Wahab, O. O., Govender, K. K., and Govender, P. P. (2025). Computational study of hydroxides of cholinium and tetramethylammonium derivatives as biofriendly ionic liquids for improved drug solubility and delivery. *Journal of Molecular Liquids*, 128954.

Wahab, O. O., Olasunkanmi, L. O., Govender, K. K., and Govender, P. P. (2018). DMol3/COSMO-RS prediction of aqueous solubility and reactivity of selected Azo dyes: Effect of global orbital cut-off and COSMO segment variation. *Journal of Molecular Liquids*, *249*, 346-360.

Wahab, O. O., Olasunkanmi, L. O., Govender, K. K., and Govender, P. P. (2020). Tuning the aqueous solubility, chemical reactivity and absorption wavelength of azo dye through systematic adjustment of molecular charge density: a DFT study. *Molecular Physics*, *118*(5), e1626508.

Waziri, I., Masena, H. M., Yusuf, T. L., Coetzee, L.-C. C., Adeyinka, A. S., and Muller, A. J. (2023). Synthesis, characterization, biological evaluation, DFT and molecular docking studies of (Z)-2-((2-bromo-4-chlorophenyl) imino) methyl)-4-chlorophenol and its Co (II), Ni (II), Cu (II), and Zn (II) complexes. *New Journal of Chemistry*, *47*(38), 17853-17870.

Waziri, I., Sookai, S., Yusuf, T. L., Olofinsan, K. A., and Muller, A. J. (2025). Exploring Anticancer Activity and DNA Binding of Metal (II) Salicylaldehyde Schiff Base Complexes: A Convergence of Experimental and Computational Perspectives. *Applied Organometallic Chemistry*, *39*(5), e70162.

Waziri, I., Yusuf, T. L., Saha, C., Sookai, S., Adeyinka, A. S., and Muller, A. J. (2025). Copper-based electrochemical sensor derived from halogen-substituted Schiff base for selective detection of neurotransmitter dopamine: Insight from DFT and docking analysis. *Results in Chemistry*, 102707.

Waziri, I., Yusuf, T. L., Zarma, H. A., Oselusi, S. O., Coetzee, L.-C. C., and Adeyinka, A. S. (2023). New palladium (II) complexes from halogen substituted Schiff base ligands: Synthesis, spectroscopic, biological activity, density functional theory, and molecular docking investigations. *Inorganica Chimica Acta*, *552*, 121505.

Weigend, F. (2006). Accurate Coulomb-fitting basis sets for H to Rn. *Physical Chemistry Chemical Physics*, *8*(9), 1057-1065.

Weigend, F., and Ahlrichs, R. (2005). Balanced basis sets of split valence, triple zeta valence and quadruple zeta valence quality for H to Rn: Design and assessment of accuracy. *Physical Chemistry Chemical Physics*, *7*(18), 3297-3305.

Xiao, Y., and Cao, C. (2018). Influence of substituent effects on the coordination ability of salicylaldehyde Schiff bases. *Journal of Coordination Chemistry*, *71*(23), 3836-3846.

Xiao, Y., and Cao, C. (2020). Influence of substituents on the structure of Schiff bases Cu (II) complexes. *Journal of Molecular Structure*, *1209*, 127916.

Zhang, H.-Z., Zhou, H.-W., Xu, P.-Y., Qin, C.-Y., Zhao, S.-Z., Li, Y.-H., and Wang, S.

(2024). The cooperative effects of ligand substituent positions and solvents on spin crossover in Mn (III) complexes based on hexadentate Schiff-base ligands. *Polyhedron*, *248*, 116757.